AN ORTHORHOMBIC DEFORMATION FAMILY OF SCHWARZ' H SURFACES

HAO CHEN AND MATTHIAS WEBER

Abstract. The classical H surfaces of H. A. Schwarz form a 1-parameter family of triply periodic minimal surfaces (TPMS) that are usually described as close relatives to his more famous P surface. However, a crucial distinction between these surfaces is that the P surface belongs to a 5-dimensional smooth family of embedded TPMS of genus three discovered by W. Meeks, while the H surfaces are among the few known examples outside this family. We construct a 2-parameter family of embedded TPMS of genus three that contains the H family and meets the Meeks family. In particular, we prove that H surfaces can be deformed continuously within the space of TPMS of genus three into Meeks surfaces.

1. Introduction

This is the second of two papers dealing with new 2-dimensional families of embedded triply periodic minimal surfaces (TPMS) of genus three whose 1-dimensional "intersections" with the well-known Meeks family exhibit singularities in the moduli space of TPMS.

Among the many TPMS discovered by H. A. Schwarz [Sch90] is a 1-parameter family H that can be constructed by extending the Plateau solution for the boundaries of the two triangular faces of a triangular prism. Such a Plateau solution does not exist for all heights of the prism. For small heights, there are two distinct solutions. One of them limits in the most symmetric singly periodic Scherk surfaces with 6 annular ends. The other degenerate to a foliation of $\mathbb{R}^3$ by horizontal parallel planes that are joined by catenoidal necks, placed in a hexagonal lattice.

This family is remarkable because it does not belong to the 5-dimensional Meeks family $\mathcal{M}$ of TPMS of genus 3 [Mee90]. Members of that family have the eight branched values of the Gauss map forming four antipodal pairs, while for an H surface, they are located at the north and south poles of the 2-sphere and the six vertices of a triangular prism. The only other known TPMS of genus 3 outside $\mathcal{M}$ are the Gyroid-Lidinoid family [Sch70, LL90, FHL93, FH99, Wey06, Wey08], and the recently discovered tΔ family [CW18].

We will exhibit a 2-parameter family oH of embedded TPMS of genus 3 that can be understood as an orthorhombic deformation family of Schwarz' H surfaces. The closure of this family has a 1-dimensional intersection with the oP family, a classical 2-parameter orthorhombic deformation family of Schwarz P surface. However, surfaces in oH are not in $\mathcal{M}$. This is, after the oΔ family in [CW18], another 2-parameter non-Meeks family of TPMS of genus 3.

Consider an embedded minimal surfaces S inside an axes parallel box $[-A, A] \times [-B, B] \times [-1, 1]$ such that

Date: July 27, 2020.

2010 *Mathematics Subject Classification.* Primary 53A10.

Key words and phrases. Triply periodic minimal surfaces.

H. Chen is supported by Individual Research Grant from Deutsche Forschungsgemeinschaft within the project "Defects in Triply Periodic Minimal Surfaces", Projektnummer 398759432.

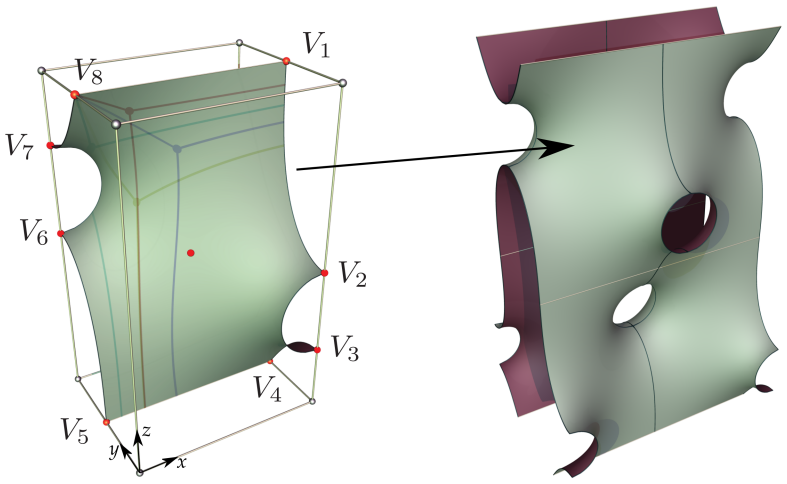

FIGURE 1.1. Fundamental Piece and Translational Fundamental Piece

- S satisfies free boundary condition on the vertical planes $x = \pm A$ and $y = \pm B$, and fixed (Plateau) boundary condition on the horizontal segments $\{(x, 0, \pm 1) \mid -A \leq x \leq A\}$.
- S intersects the edges of the box in eight vertices, but disjoint from the vertical lines with $(x, y) = \pm(+A, +B)$. Hence, apart from the four ends of the fixed boundaries, S intersects the vertical lines $(x, y) = \pm(+A, -B)$ in two vertices each.
- S is symmetric under the inversion in the origin.

Therefore S is a right-angled minimal octagon, with its inversion center at the origin. See Figure 1.1 (left) for an example. If the vertices are labeled as in this figure, then the fixed boundaries are the segments V_8V_1 and V_4V_5.

Because the two horizontal segments are in the middle of the top and bottom faces of the box, rotations about them and reflections in the lateral faces of the box extend S to a TPMS $\tilde{\Sigma}$. More specifically, $\tilde{\Sigma}$ is invariant under the lattice Λ spanned by $(2A, 0, 2)$, $(-2A, 0, 2)$ and $(0, 4B, 0)$. In the 3-torus $\mathbb{R}^3/\Lambda$, $\Sigma = \tilde{\Sigma}/\Lambda$ is a compact surface of genus 3. In Figure 1.1 (right) we show part of $\tilde{\Sigma}$ consisting of eight copies of S.

Remark 1.1. For crystallographers, the orthorhombic lattice spanned by $(4A, 0, 0)$, $(0, 4B, 0)$ and $(0, 0, 4)$ is probably more convenient. This is responsible for the letter "o" in our naming. The part shown in Figure 1.1 (right) is actually a translational fundamental domain of this orthorhombic lattice. The quotient of $\tilde{\Sigma}$ by this lattice is a double cover of Σ, hence of genus 5.

We use $\mathcal{O}$ to denote the set of all TPMS obtained in this way. Two classical families of surfaces in $\mathcal{O}$ were already known to Schwarz [Sch90].

Surfaces in the first family have an additional reflectional symmetry in the plane $z = 0$. Then, because of the inversional symmetry in the origin, these surfaces must also contain the z-axis, which serves as the axis of an order-2 rotational symmetry. This 2-parameter family contains Schwarz' P surface and belongs to the Meeks' family $\mathcal{M}$ [Mee90]. It is known as oPb in the literature to distinguish from another orthorhombic deformation family oPa; see [FK89, FH92]. In this paper, we simply write oP in place of oPb. An example of oP with small B is shown in Figure 1.2 (left).

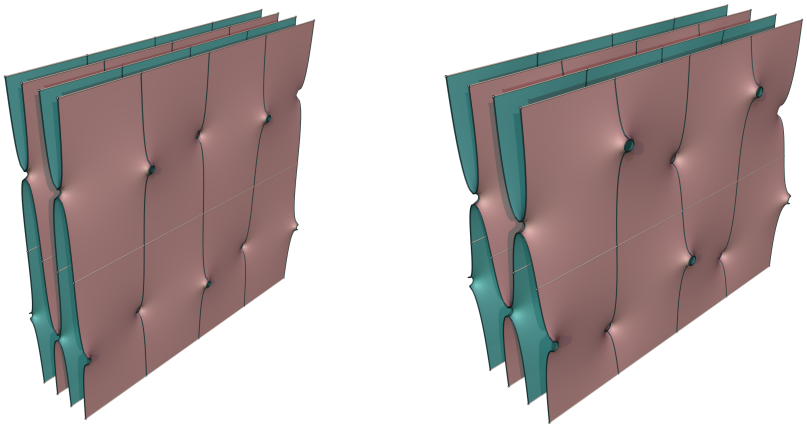

FIGURE 1.2. Surfaces in oP and H near catenoidal limits

Surfaces in the second family have an additional order-3 rotational symmetry about a line in the y-direction. The rotational axis necessarily passes through an end of fixed boundary. This 1-parameter family is Schwarz' H family. An example, again with small B, is shown in Figure 1.2 (right).

The main purpose of this paper is to establish the existence of a new 2-parameter family described in the following theorem, and study its properties.

Theorem 1.2. *There exists a 2-parameter continuous family* oH *in* $\mathcal{O}$ *that contains Schwarz'* H *surfaces as a subfamily. Surfaces in* oH *do not belong to the Meeks family. That is, the branched values of the Gauss map do not form four antipodal pairs. In fact, the only Meeks surfaces in* $\mathcal{O}$ *are the* oP *surfaces. However, the closure of* oH *intersects* oP *in a* 1*-parameter family of TPMS.*

The intersection $\overline{\text{oH}} \cap \text{oP}$ will be explicitly described in terms of elliptic integrals.

We now provide the motivation that leads to the discovery of oH.

By opening nodes among 2-tori, Traizet [Tra08] constructed TPMS that looks like horizontal planes connected by catenoidal necks. In the degenerate limit, the catenoidal necks become nodes whose positions have to satisfy a balancing equation, formulated in terms of elliptic functions, and a non-degeneracy condition.

For surfaces of genus 3, one needs to open two nodes between two tori. In the limit, it degenerates to a two-sheeted torus with two singular points. Let $(T_1, T_2) \in \mathbb{C}^2$ be vectors that span the limit torus, and write $T_3 = -T_1 - T_2$. Assume that limit positions of the two nodes are p_1 and p_2, respectively. Up to a translation, we may assume that $p_1 = 0$. Write $p_2 = xT_1 + yT_2$ with $(x, y) \in [0, 1]^2$. Then p_1, p_2 form a balance configuration if (see [Tra08, §4.3.3])

$$\zeta(p_2) = x\eta_1 + y\eta_2 \ , \tag{1.1}$$

where ζ is Weierstrass Zeta function, which is quasi-periodic in the sense that $\zeta(z + T_i) - \zeta(z) = \eta_i = 2\zeta(T_i/2)$, $i = 1, 2, 3$. Traizet proved that, if such a balanced configuration is non-degenerate, then there exists a family of triply periodic minimal surfaces that limits in this configuration.

Remark 1.3. If we follow [Tra08] more closely, we would need to consider an infinite sequence of tori indexed by $\mathbb{Z}$, and open a node between each adjacent pair under the periodicity assumption that $p_{k+2} = p_k + T$ for some $T \in \mathbb{C}$. The current

paper only deals with the monoclinic special case with $T = 0$, hence the simplified formulation.

Recall that $\eta_1 + \eta_2 + \eta_3 = 0$. Hence for any T_1 and T_2, there are three trivial balanced configurations, given by $(x, y) = (1/2, 1/2)$, $(0, 1/2)$ and $(1/2, 0)$, respectively. In other words, if p_2 is a 2-division point, the balance equation is automatically solved for any torus. In particular, when $|T_1| = |T_2|$, the configuration $x = y = 1/2$ is the Traizet limit of the oP (oPb) family; when T_2/T_1 is purely imaginary, the configuration $x = y = 1/2$ is the Traizet limit of the oPa family, and the configuration $(x, y) = (0, 1/2)$ (or $(1/2, 0)$) is the Traizet limit of an orthorhombic deformation family of CLP surfaces (termed oCLP' in [FH92]). Another special case is the rhombic 60° torus. The hexagonal symmetry implies two non-trivial balanced configurations with $x = y = 1/3$ and $x = y = 2/3$, which is the Traizet limit of the H family (non-Meeks). Traizet limit of these classical TPMS are illustrated in Figure 1.3.

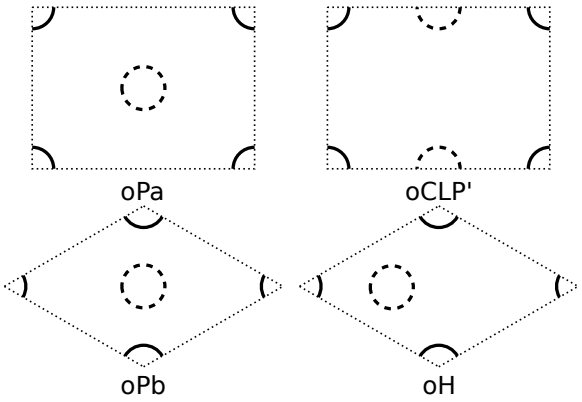

FIGURE 1.3. Balanced configurations that give Traizet limits of classical families of TPMS. The solid circle is centered at p_1 and the dashed circle is centered at p_2.

More generally, we consider on rhombic tori spanned by $T_{1,2} = \exp(\pm i\theta/2)$ the balanced configurations with $x = y$. The symmetry suggests that these are Traizet limit of $\mathcal{O}$ surfaces with $B \to 0$. To see this, just rotate the configuration to place T_3 in the z-direction and open nodes in the y-direction. The balance equation for such a configuration is given by

$$x\zeta(T_3/2) = \zeta(xT_3)/2 \tag{1.2}$$

Our choice of conjugate vectors T_1, T_2 guarantees real values on both sides. The solution set to this balanced equation is shown in Figure 1.4. The vertical line $x = 1/2$ is the trivial locus, giving the Traizet limit of the oP surfaces.

But we also see a second, non-trivial locus, which is the motivation of the current project. This "exotic" locus has been noticed independently by both authors, and probably by many other people in the minimal surface community. We will see that balanced configurations on this locus are all non-degenerate, so they are indeed Traizet limits. In fact, they are the Traizet limits of the oH family. Our discovery of oH is actually the result of an attempt to push TPMS away from these Traizet limits.

The two loci of Traizet limits intersect at $x = 1/2$ and $\theta = \theta^* \approx 1.23409 \approx 70.7083°$. The balanced configuration at the intersection is degenerate.

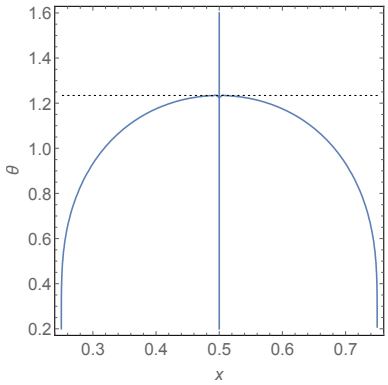

FIGURE 1.4. Solution set (x, θ) to the balance equation (1.2) on the diagonal of rhombic tori. The dotted horizontal line mark the position of θ^*.

The torus $\mathbb{T}^*$ at the intersection is of particular significance. It is the only rhombic torus on which there exists a meromorphic 1-form with double order pole at 0 and double order 0 at $T_3/2$ and only real periods. This was exploited for the construction of translation invariant helicoids with handles [HKW99, WHW09]. This meromorphic 1-form can be constructed geometrically as follows (see Figure 1.5): Take the complex plane, and slit it along the interval $[-1, 1]$ on the real axis. Then identify the top (resp. bottom) edge of $[-1, 0]$ with the bottom (resp. top) edge of $[0, 1]$. The result is a torus carrying a cone metric with two cone points, of cone angle 6π at the point identified with $\{-1, 0, 1\}$, and of cone angle -2π at ∞. The corresponding 1-form has thus a double order pole at 0, and a doubly order zero at ∞. Its periods are obviously real, and the symmetry of the slit ensures that the torus is rhombic. The same torus with flat metric is nothing but $\mathbb{T}^*$.

We will revisit the Traizet limit in Section 6 in the framework of our parametrization of oH. We first prove that the non-trivial locus is non-degenerate, and unique in the sense that for every $0 < \theta < \theta^*$, (1.2) has a unique solution $0 < x < 1/2$. Then (1.2) will be reformulated in terms of elliptic integrals, leading to an explicit formula for the non-trivial locus. We will also recover θ^*, not only as the end point of the Traizet limit of oH, but also as the Traizet limit of the intersection $\overline{\text{oH}} \cap \text{oP}$.

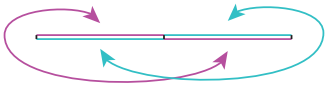

FIGURE 1.5. Model for the torus $\mathbb{T}^*$

Our paper is organized as follows:

In Section 2, we describe the Weierstrass data for surfaces in $\mathcal{O}$, prove their embeddedness, and formulate the period problem, depending on three real positive parameters a, b and t. The case $a = b$ corresponds to the oP surfaces, where the period problem is automatically solved. In the case $a \neq b$, the period problem becomes 1-dimensional.

In Section 3 we show that, if $a \neq b$, the branched values of the Gauss map can *not* be antipodal. This proves that $\mathcal{O} \cap \mathcal{M} = \text{oP}$, and that any solution with $a \neq b$ (namely oH) lies outside $\mathcal{M}$.

Section 4 is dedicated to the existence proof of oH. We show that for any choice of $a \neq b$, there is a value of t that solves the period problem. This is accomplished through a careful asymptotic analysis of the period integrals. We also conjecture the uniqueness of t based on numerical experiments.

To prove that oP and the closure of oH have a non-empty intersection, we consider in Section 5 a modified period problem that eliminates the trivial solutions coming from oP. It turns out that the intersection can be explicitly described in terms of elliptic integrals.

In section 6 we study the Traizet limit of oH. In particular, the loci of (1.2) will receive another explicit description in terms of elliptic integrals, and the intersection of the loci will be recovered in two different ways. We also locate the Traizet limit of H family on the locus. It is then possible to find a continuous deformation path within the space of TPMS of genus three, starting from an H surface and ending with an oP surface, that passes through a sufficiently small neighborhood of the Traizet limit.

Despite different appearances, motivations and focus points, our parametrization of oH, as well as many computations, share similarities with our previous work on oΔ [CW18]. So we will, whenever appropriate, refer the readers to [CW18] for details. We also omit technical details in Sections 5 and 6, where integral tables in [BF71] are used for the computations involving elliptic integrals.

Acknowledgements. We are grateful to the anonymous referee for suggestions and corrections after carefully reading a previous version of the manuscript.

2. Weierstrass Data and the Period Problem

We parameterise a surface in $\mathcal{O}$ using a Weierstrass representation defined on the upper half plane such that the real axis is mapped to the boundary of the octagon S. Let the vertices of S be labeled by $V_1, V_2, \cdots, V_8$ as in Figure 1.1 (left). Denote the preimage of V_k by $v_k \in \mathbb{R}$, and assume that $v_1 < v_2 < \ldots < v_8$.

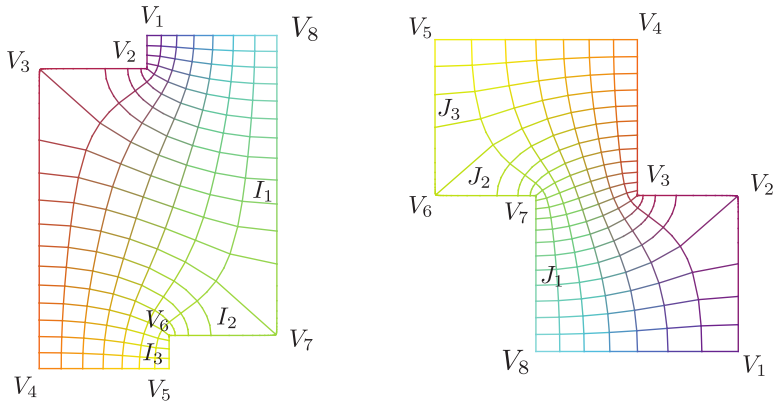

Figure 2.1. Images of a fundamental piece under Φ_1 and Φ_2.

Given an $\mathcal{O}$ surface, denote by dh its height differential and by G its Gauss map. Let $\phi_1 := dh \cdot G$ and $\phi_2 := dh/G$. The assumed boundary symmetries of the surface imply that $\Phi_j : z \mapsto \int^z \phi_j$ ($j = 1$ or 2) map the upper half plane to "right angled" Euclidean octagons. The interior angle is $270°$ at $\Phi_1(v_2)$, $\Phi_1(v_6)$ and $\Phi_2(v_3)$, $\Phi_2(v_7)$. Indeed, the Gauss map is vertical at V_2, V_3, V_6 and V_7, hence these vertices are the poles and the zeros of G. Interior angles at all other vertices are $90°$; see Figure 2.1.

We may assume that the inversion is represented by the transform $\iota : z \mapsto -1/z$, hence the inversion center of the minimal octagon at the origin is represented by i in the upper half plane. Then we assume the eight points v_i to be $-t < -a < -1/b < -1/t < 1/t < 1/a < b < t$ for $t > 1$.

Such maps are given by Schwarz-Christoffel maps. More specifically, we have

$$\begin{aligned}\phi_1 &:= -\rho\,\frac{(z+a)^{+1/2}(z+1/b)^{-1/2}(z-1/a)^{+1/2}(z-b)^{-1/2}}{(z+t)^{1/2}(z+1/t)^{1/2}(z-1/t)^{1/2}(z-t)^{1/2}}\,dz,\\ \phi_2 &:= \frac{1}{\rho}\,\frac{(z+a)^{-1/2}(z+1/b)^{+1/2}(z-1/a)^{-1/2}(z-b)^{+1/2}}{(z+t)^{1/2}(z+1/t)^{1/2}(z-1/t)^{1/2}(z-t)^{1/2}}\,dz,\\ dh &:= \frac{i}{(z+t)^{1/2}(z+1/t)^{1/2}(z-1/t)^{1/2}(z-t)^{1/2}}\,dz\ .\end{aligned}$$

Here, the real positive Lopéz-Ros factor ρ determines the scaling of the image domains. The Gauss map is given by

$$G(z) = i\rho(z-1/a)^{+1/2}(z+a)^{+1/2}(z+1/b)^{-1/2}(z-b)^{-1/2}\ .$$

Proposition 2.1. *Up to congruence and dilation, the image of the upper half plane under the map*

$$F : z \mapsto \operatorname{Re}\int^z (\omega_1,\omega_2,\omega_3) = \operatorname{Re}\int^z \left(\frac{1}{2}(\phi_2-\phi_1), \frac{i}{2}(\phi_2+\phi_1), dh\right) \tag{2.1}$$

is almost *the fundamental octagon of an $\mathcal{O}$ surface in the following sense:*

- *The intervals v_8v_1 and v_4v_5 are mapped to straight segments in the x-direction, but not necessarily in the $y = 0$ plane.*
- *The other intervals are mapped to planar symmetry curves in vertical planes. More specifically:*
  - *the interval v_1v_2 (resp. v_5v_6) is mapped into the plane $x = +A$ (resp. $-A$);*
  - *the interval v_2v_3 (resp. v_6v_7) is mapped into the plane $y = -B$ (resp. $+B$);*
  - *the interval v_3v_4 (resp. v_7v_8) is mapped into the plane $x = +A'$ (resp. $-A'$).*
- *The image is symmetric under the inversion ι in the image of i.*

The proof is a straightforward modification of the proof in [CW18].

Proposition 2.2. *All minimal octagons constructed by Proposition 2.1 are embedded. In particular, the triply periodic minimal surfaces in $\mathcal{O}$, generated by extending the octagon across symmetry lines, are embedded as well.*

Proof. We note that the space $\mathcal{S}$ of these octagons is parametrized by the parameters a, b, t and ρ, and hence connected. Moreover, $\mathcal{S}$ contains known embedded surfaces, namely the oP and H surfaces of H.A. Schwarz.

Now let Σ_1 be an arbitrary surface in $\mathcal{S}$, and connect it continuously to an embedded surface Σ_0 in $\mathcal{S}$. Let Σ be the first surface in this family that is not embedded anymore. We denote by $\partial\Sigma = F(\mathbb{R}\cup\{\infty\})$ the boundary of Σ, while $\Sigma = F(\mathbb{R}\times\mathbb{R}^+)$ denotes the interior. By the maximum principle, the immersion fails to be embedded at a boundary point of Σ.

The boundary $\partial\Sigma$ itself is parametrized by F injectively: On the vertical segments between V_5 and V_8 and between V_1 and V_4, this follows because the height differential is real with constant sign. The straight horizontal segments are parametrized injectively because the parametrization is conformal and non-degenerate.

Thus it remains to show that the $\partial\Sigma$ cannot meet a point of Σ. This is clear for most boundary segments V_iV_{i+1} by the convex hull property of minimal surface.

But this argument could fail when the arc V_7V_8 is not coplanar with the arc V_5V_6, i.e. when $A \neq A'$. If $A' < A$, for instance, then there could be an interior point p_0 of Σ that meets V_7V_8. If this is the case, Σ would be tangential to $\partial\Sigma$ at p_0.

By the explicit expression of the Gauss map, no point of Σ has a normal vector parallel to the xz-plane, hence the tangent plane cannot be parallel to the y-direction. It is therefore possible to find a curve $\gamma(t)$ on Σ, starting from p_0, whose tangent vector is in the direction of $(-1, y(t), 1)$. This curve can only terminate at a boundary point of $\partial\Sigma$ or at an interior point with a tangent plane containing the y-direction. The latter doesn't exist, and there is no component of the boundary having points with smaller x-coordinate and greater z-coordinate than V_7. This contradiction shows that $\bar{\Sigma} = \Sigma \cup \partial\Sigma$ is embedded. □

For such a minimal octagon to lie in $\mathcal{O}$, we must have have $A = A'$ so that the curves V_1V_2 and V_3V_4 are coplanar, hence the image of (2.1) is contained in an axis parallel box centered at the origin. Moreover, V_8V_1 and V_4V_5 must lie in the middle of, respectively, the top and bottom faces of the box. We now express these conditions in terms of the periods of ϕ_1 and ϕ_2. To this end, we introduce notations for the edge lengths of the Euclidean octagons

$$I_k := \left| \int_{v_k}^{v_{k+1}} \phi_1 \right|, \qquad J_k := \left| \int_{v_k}^{v_{k+1}} \phi_2 \right|$$

for $1 \leq k \leq 7$. These are positive real numbers that depend analytically on the parameters a, b, t and ρ. Note that by the inversional symmetry, we have

$$I_k = I_{k+4} \quad \text{and} \quad J_k = J_{k+4} \tag{2.2}$$

for $1 \leq k \leq 3$.

Proposition 2.3. *The image of the upper half plane under the Weierstrass representation* (2.1) *is the fundamental octagon of a surface in $\mathcal{O}$ if and only if the following period conditions are satisfied:*

$$\begin{aligned} I_1 + I_3 &= J_1 + J_3 \ , \\ I_2 &= J_2 \ . \end{aligned} \tag{2.3}$$

Proof. The curves V_1V_2 and V_3V_4 are coplanar if and only if

$$\mathrm{Re} \int_{v_2}^{v_3} \omega_1 = 0 \ .$$

This is equivalent to

$$\mathrm{Re} \int_{v_2}^{v_3} (\phi_1 - \phi_2) = 0.$$

Observe that on v_2v_3, the integrands of ϕ_1 and ϕ_2 are both negative real. So the equation above can be written as $I_2 = J_2$, which is the second period condition.

The top segment V_8V_1 lies in the middle of the top face if and only if

$$\mathrm{Re} \int_{v_1}^{v_2} \omega_2 = \mathrm{Re} \int_{v_7}^{v_8} \omega_2 \ .$$

This is equivalent to

$$\mathrm{Im} \int_{v_1}^{v_2} (\phi_1 + \phi_2) = \mathrm{Im} \int_{v_7}^{v_8} (\phi_1 + \phi_2) \ .$$

Observe on v_1v_2 that the integrand in ϕ_1 (resp. ϕ_2) is negative (resp. positive) imaginary, and on v_7v_8 that the integrand in ϕ_1 (resp. ϕ_2) is positive (resp. negative) imaginary. So the equation above can be written as

$$I_1 - J_1 = J_7 - I_7 = J_3 - I_3,$$

where the second equation follows from the symmetry (2.2). This proves the first period condition.

If the period conditions are satisfied, then by the inversional symmetry ι, the curves V_5V_6 and V_7V_8 must also be coplanar, and the segment V_4V_5 must also lie in the middle of the bottom box. □

We can eliminate ρ by taking the quotient of the two equations, therefore:

Corollary 2.4. *If*

$$Q_I := \frac{I_1 + I_3}{I_2} = \frac{J_1 + J_3}{J_2} =: Q_J$$

or, equivalently, if

$$Q := Q_I - Q_J = \frac{I_1 + I_3}{I_2} - \frac{J_1 + J_3}{J_2} = 0 \tag{2.4}$$

for some choice of a, b, t, then $\rho \in \mathbb{R}_{>0}$ can be uniquely adjusted so that the period conditions (2.3) *are satisfied.*

Thus we have expressed the period condition as a single equation $Q = 0$, where Q depends on three parameters a, b, t.

Note that when $a = b$, we have additional symmetries:

The involution $\sigma_1 : z \mapsto -\overline{z}$ transforms the Weierstrass data by

$$\sigma_1^* dh = \overline{dh(z)} \quad \text{and} \quad G(\sigma_1(z))\overline{G(z)} = \rho^2.$$

Consequently, we have $I_k = \rho^2 J_{4-k}$ for $1 \le k \le 3$, so the period conditions (2.3) are satisfied automatically with $\rho = 1$. In this case, it can be explicitly verified that the positive imaginary axis is mapped by the Weierstrass representation (2.1) to the vertical straight segment between the middle points of V_4V_5 and V_8V_1, and σ_1 induces an order-2 orientation-reversing rotation of the surface around this segment.

On the other hand, the involution $\sigma_2 : z \mapsto 1/\overline{z}$ induces an order-2 reflection in the $z = 0$ plane. This can be seen by observing that $\sigma_1 \circ \sigma_2 = \iota$.

To simplify our computations in the following sections, we employ the substitution $\zeta = z - 1/z$, which is monotone on the positive real axis. We also replace $a - 1/a$ by α, $b - 1/b$ by β, and $t - 1/t$ by τ so that $-\tau < -\alpha < \beta < \tau$. Then the 1-forms ϕ_1 and ϕ_2 become

$$\begin{aligned}
\phi_1 &= -\rho(\zeta + \alpha)^{+1/2}(\zeta - \beta)^{-1/2}(\zeta^2 - \tau^2)^{-1/2}(\zeta^2 + 4)^{-1/2}\, d\zeta\ , \\
\phi_2 &= \frac{1}{\rho}(\zeta + \alpha)^{-1/2}(\zeta - \beta)^{+1/2}(\zeta^2 - \tau^2)^{-1/2}(\zeta^2 + 4)^{-1/2}\, d\zeta\ ,
\end{aligned}$$

and the Gauss map is simplified to

$$G(\zeta) = \rho i(\zeta + \alpha)^{+1/2}(\zeta - \beta)^{-1/2}. \tag{2.5}$$

In the rest of the paper, the original parametrization is understood whenever Latin letters a, b, t, z are used, and the simplified parametrization is understood whenever Greek letters $\alpha, \beta, \tau, \zeta$ are used. This should not cause any confusion.

3. Branched Values of the Gauss Map

In this section, we will show that the branched values of the Gauss map are never antipodal with $a \neq b$. As a consequence, the only surfaces in $\mathcal{O}$ that belong to the Meeks family $\mathcal{M}$ are the surfaces in oP. The arguments don't require the period condition to be satisfied and are purely algebraic.

Theorem 3.1. *The branched values of the Gauss map of a surface in $\mathcal{O}$ are antipodal if and only if $a = b$.*

Proof. We begin by locating the branched points of the Gauss map in the fundamental octagon. By a result of Meeks [Mee90], the branched points of a TPMS of genus 3 are precisely the inversion centers of the surface. They are situated, in the fundamental octagon, at the center of the octagon and at the end points of the fixed boundary segments.

The octagon center corresponds to i in the upper half plane, so that $G(i)$ is a branched value. Three more branched points and values are obtained after extending the octagon by reflections. We then have four branched values, namely $\pm G(i)$ and $\pm\overline{G(i)}$. Their stereographic images on the 2-sphere lie at the vertices of a horizontal rectangle, symmetric in the planes $x = 0$ and $y = 0$.

The end points of the fixed boundary segments correspond to $\pm t$ and $\pm 1/t$ in the parameter domain. Because of the inversional symmetry, they provide only two branched values $G(t)$ and $G(-t)$. These both lie on the positive imaginary axis, and their stereographic images on the 2-sphere lie on the upper half-circle with $y > 0$ and $x = 0$. Extending the octagon by reflections gives two more branched values at $-G(t)$ and $-G(-t)$, whose stereographic images lie on the lower half-circle. The stereographic images of these four branched values then form a quadrilateral in the plane $x = 0$ symmetric to the plane $y = 0$.

We show an example for the location of the eight branched values in Figure 3.1.

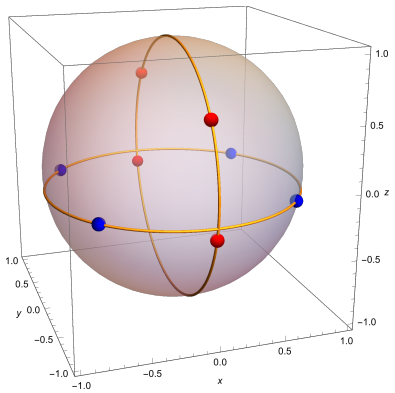

FIGURE 3.1. Branched values of the Gauss map

In order that these eight branched values occur in antipodal pairs, the first quadrilateral must lie in the plane $z = 0$, while the second quadrilateral must be a rectangle. These conditions mean, in terms of the Gauss map, that $|G(i)| = 1$ and $G(t)G(-t) = -1$. We then compute from (2.5) that

$$\rho^2\sqrt{\frac{\alpha^2+4}{\beta^2+4}} = 1 \quad \text{and} \quad \rho^2\sqrt{\frac{\tau^2-\alpha^2}{\tau^2-\beta^2}} = 1,$$

which forces $\alpha = \pm\beta$, hence $a = b$ under the constraint $1/t < 1/a < b < t$. □

The reader might be curious about the parameter values for the Schwarz H surfaces within this representation. These are difficult to determine explicitly. But we know that, among the eight branched values of the Gauss map of an H surface, there is one and only one antipodal pair. This implies either $G(t) = G(-1/t) = i$ or $G(-t) = G(1/t) = i$. We then obtain from (2.5) a necessary condition of the parameters for H, namely

$$\rho^2\frac{\tau+\alpha}{\tau-\beta} = 1 \quad \text{or} \quad \rho^2\frac{\tau-\alpha}{\tau+\beta} = 1.$$

In view of Conjecture 4.3 in the next section, we believe that this condition is also sufficient.

We see from (2.5) that, for any reals α, β, ρ with $-\alpha < \beta$ and $\rho > 0$, there is a unique $\zeta^* \in (\infty, -\alpha) \cup (\beta, \infty) \cup \infty$ such that $G(\zeta^*) = i$. In other words, there must be a point on the boundary of the octagon, namely the image of ζ^* under (2.1), where the normal vector points in the y direction. For the oP family, $\rho = 1$ and $\alpha = \beta$, hence $\zeta^* = \infty$. For the H family, our calculation above shows that $\zeta^* = \pm\tau$. So $\mathcal{O}$ is divided in two parts, depending on the image of ζ^* being on the fixed boundary (as oP) or on the free boundary of the octagon; Schwarz H family lies on the interface.

Remark 3.2. Using the order-3 rotational symmetry of the H surfaces, a computer algebra system gives the explicit expressions

$$\alpha = \tau \frac{4(\tau^2+4)\sqrt{\tau^4 - 56\tau^2 + 16} - (3\tau^4 - 40\tau^2 + 48)}{7\tau^4 + 88\tau^2 - 16}$$
$$\beta = \tau \frac{4(\tau^2+4)\sqrt{\tau^4 - 56\tau^2 + 16} + (3\tau^4 - 40\tau^2 + 48)}{7\tau^4 + 88\tau^2 - 16}$$

for the parameters α and β in terms of τ. Then the period problem seems automatically solved, at least numerically.

4. Existence of Non-Trivial Solutions

Recall that $0 < 1/t < 1/a < b < t$, and the periodic condition (2.4) as we copy below

$$Q(a, b; t) = \frac{I_1 + I_3}{I_2} - \frac{J_1 + J_3}{J_2} = 0.$$

The quantity Q is our focus in the remaining sections of this paper. From now on, we will ignore the Lopéz-Ros factor ρ in our calculations, since Q is independent of this factor.

We now prove the main theorem of this paper.

Theorem 4.1. *If $a = b$, the period condition* (2.4) *is solved for any choice of t.*
If $a < b$, then there exists a value of t that solves the period condition (2.4)*.*

The case $a = b$ has been discussed in Section 2. The case $a < b$, as well as the existence of oH, follows from the continuity of Q in t, and the following proposition.

Proposition 4.2. *If $1/t < 1/a < b < t$ and $a < b$ then*

$$\lim_{t \to b+} Q(a, b; t) < 0 \ , \tag{4.1}$$

$$\lim_{t \to +\infty} Q(a, b; t) = +\infty \ . \tag{4.2}$$

The remainder of this section is devoted to the proof of this proposition.

Proof of (4.1). The argument in [CW18] applies with slight modification. As $t \to b+$, all periods have finite positive limits, with the exceptions $\lim_{t\to b+} J_3 = 0$ and $\lim_{t\to b+} I_2$ diverges to $+\infty$. Thus

$$\lim_{t \to b+} \frac{I_1 + I_3}{I_2} = 0 \quad \text{and} \quad \lim_{t \to b+} \frac{J_1 + J_3}{J_2} > 0 \ ,$$

and (4.1) follows. □

Proof of (4.2). The proof is similar to the argument in [CW18]. Recall that the substitution $\zeta = z - 1/z$ is monotonically increasing for $z > 0$, and write $\alpha = a - 1/a$, $\beta = b - 1/b$, $\tau = t - 1/t$ as before.

For the periods in the denominators, we first note that

$$\lim_{\tau\to\infty} \tau\cdot I_2(\alpha,\beta;\tau) = \int_{-\alpha}^{\beta} \frac{1}{\sqrt{\zeta^2+4}}\sqrt{\frac{\alpha+\zeta}{\beta-\zeta}}\,d\zeta,$$
$$\lim_{\tau\to\infty} \tau\cdot J_2(\alpha,\beta;\tau) = \int_{-\alpha}^{\beta} \frac{1}{\sqrt{\zeta^2+4}}\sqrt{\frac{\beta-\zeta}{\alpha+\zeta}}\,d\zeta$$

are all finite. Their difference

$$\begin{aligned}\lim_{\tau\to\infty} \tau\cdot(I_2-J_2) &= \int_{-\alpha}^{\beta} \frac{2\zeta+\alpha-\beta}{\sqrt{(\zeta^2+4)(\alpha+\zeta)(\beta-\zeta)}}\,d\zeta\\ &= \int_{-\gamma}^{\gamma} \frac{2\xi\,d\xi}{\sqrt{((\xi-\alpha/2+\beta/2)^2+4)(\gamma^2-\xi^2)}}\\ &= \int_0^{\gamma} \frac{2\xi\,d\xi}{\sqrt{\gamma^2-\xi^2}}\Big(\frac{1}{\sqrt{(\xi-\alpha/2+\beta/2)^2+4}} - \frac{1}{\sqrt{(\xi+\alpha/2-\beta/2)^2+4}}\Big),\end{aligned}$$

where $\gamma=(\alpha+\beta)/2$ and $\xi=\zeta-(\beta-\alpha)/2$, is negative when $\alpha<\beta$. Hence we have

$$\lim_{\tau\to\infty} \tau I_2 < \lim_{\tau\to\infty} \tau J_2 \tag{4.3}$$

for all $0<\alpha<\beta$.

The periods in the numerators have logarithmic asymptotics. For instance, as $\tau\to\infty$,

$$\begin{aligned}\tau\cdot J_3(\alpha,\beta;\tau) &= \int_{\beta}^{\tau} \frac{\tau}{\sqrt{\zeta^2+4}\sqrt{\tau^2-\zeta^2}}\sqrt{\frac{\zeta-\beta}{\zeta+\alpha}}\,dz\\ &\sim \int_{\beta}^{\tau} \frac{\tau}{\zeta\sqrt{\tau^2-\zeta^2}}\,d\zeta\\ &\sim \log t,\end{aligned}$$

hence $\tau\cdot I_3(\alpha,\beta;\tau)$ diverges to $+\infty$ as $\tau\to\infty$. Fortunately, the integrals I_1 and J_1 (and I_3 and J_3) have the same logarithmic singularities. By the dominated convergence theorem, we obtain the following limits:

$$\begin{aligned}\lim_{\tau\to\infty} \tau\cdot(I_1-J_1) &= -\lim_{\tau\to\infty}\int_{-\tau}^{-\alpha} \frac{\tau(\alpha+\beta)}{\sqrt{(\tau^2-\zeta^2)(\zeta^2+4)(\beta-\zeta)(-\alpha-\zeta)}}\,d\zeta\\ &= -\int_{-\infty}^{-\alpha} \frac{\alpha+\beta}{\sqrt{\zeta^2+4}\sqrt{\beta-\zeta}\sqrt{-\alpha-\zeta}}\,d\zeta,\\ \lim_{\tau\to\infty} \tau\cdot(I_3-J_3) &= \lim_{\tau\to\infty}\int_{\beta}^{\tau} \frac{\tau(\alpha+\beta)}{\sqrt{\tau^2-\zeta^2}\sqrt{\zeta^2+4}\sqrt{\zeta-\beta}\sqrt{\zeta+\alpha}}\,d\zeta\\ &= \int_{\beta}^{\infty} \frac{\alpha+\beta}{\sqrt{\zeta^2+4}\sqrt{\zeta-\beta}\sqrt{\zeta+\alpha}}\,d\zeta.\end{aligned} \tag{4.4}$$

Note that both integrals are finite and non-zero.

Finally, we write

$$Q(\alpha,\beta;\tau) = \frac{\tau(I_1-J_1)+\tau(I_3-J_3)}{\tau I_2} + \tau(J_1+J_3)\Big[\frac{1}{\tau I_2}-\frac{1}{\tau J_2}\Big].$$

The part in the square bracket is positive by (4.3). As $\tau\to\infty$, the first fraction is finite by (4.4), and $\tau(J_1+J_3)\to+\infty$. This concludes the proof of the proposition. □

Before ending this section, we propose the following uniqueness conjecture based on numeric experiments:

Conjecture 4.3. *If $a < b$, then there exists a unique t that solves the period condition* (2.4).

5. Intersection with the Meeks-Locus

We show in this section that $\overline{\text{oH}}$ intersects oP in a 1-parameter family. To make this precise, we use on $\mathcal{O}$ the topology induced by the space of possible Weierstrass data, which are determined by the four real parameters a, b, t and ρ. Clearly, the convergence of Weierstrass data implies the locally uniform convergence of the minimal surfaces.

The goal is to explicitly determine the intersection of the Meeks locus

$$\text{oP} = \{(a, b, t) : Q(a, b; t) = 0, a = b, 0 < 1/t < 1/a < b < t\}$$

with the closure of the non-Meeks locus

$$\text{oH} = \{(a, b, t) : Q(a, b; t) = 0, a \neq b, 0 < 1/t < 1/a < b < t\}.$$

Without loss of generality, we will focus on the case $a < b$ hence $\alpha < \beta$. The idea is to divide the function $Q(\alpha, \beta; \tau)$ by $\beta - \alpha$ and take the limit for $\alpha \to \beta-$ to eliminate solutions in the Meeks locus. We claim:

Theorem 5.1. *The intersection $\overline{\text{oH}} \cap \text{oP}$ is described by the equation*

$$\bar{K}(m_1)E(m_2) + m_2\bar{E}(m_1)K(m_2) = \bar{K}(m_1)K(m_2), \tag{5.1}$$

where

$$K(m) = \int_0^{\pi/2} \frac{1}{\sqrt{1 - m\sin^2(\theta)}}\, d\theta,$$

$$E(m) = \int_0^{\pi/2} \sqrt{1 - m\sin^2(\theta)}\, d\theta$$

are complete elliptic integrals of the first and the second kind, $\bar{K}(m) = K(1 - m)$ and $\bar{E}(m) = E(1 - m)$ are the associated elliptic integrals, using the moduli

$$m_1 = \frac{\alpha^2 + 4}{\tau^2 + 4}, \qquad m_2 = \frac{\alpha^2}{\tau^2}\frac{\tau^2 + 4}{\alpha^2 + 4}.$$

Note that $0 < m_1, m_2 < 1$.

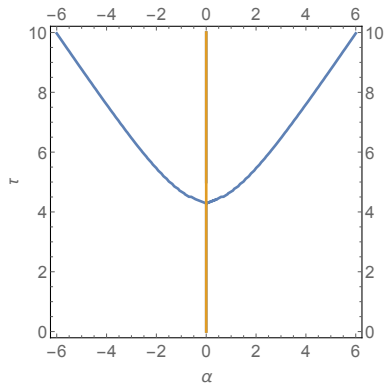

FIGURE 5.1. Solution set (α, τ) to the period condition (5.1) describing the intersection $\overline{\text{oH}} \cap \text{oP}$.

The theorem follows from the following proposition:

Proposition 5.2. *The function*

$$\tilde{Q}(\alpha,\beta;\tau)=\frac{Q(\alpha,\beta;\tau)}{\beta-\alpha}$$

extends analytically to $\alpha=\beta$ by

$$\tilde{Q}(\alpha,\alpha;\tau)=\frac{\tau^2}{\alpha^2}\frac{\tau}{\tau^2-\alpha^2}\sqrt{\frac{\alpha^2+4}{\tau^2+4}}\frac{\bar{K}(m_1)E(m_2)+m_2\bar{E}(m_1)K(m_2)-\bar{K}(m_1)K(m_2)}{K(m_2)^2}.$$

Proof. With the help of the integral tables in [BF71], we obtain the following explicit evaluation of the periods.

$$(I_1+I_3)(\alpha,\alpha;\tau)=(J_1+J_3)(\alpha,\alpha;\tau)=\frac{2}{\sqrt{\tau^2+4}}\bar{K}(m_1)\ ,$$
$$I_2(\alpha,\alpha;\tau)=J_2(\alpha,\alpha;\tau)=\frac{\alpha}{\tau}\frac{2}{\sqrt{\alpha^2+4}}K(m_2)\ .$$

Then we evaluate the derivatives

$$I_k'(\alpha,\alpha;\tau)=\frac{\partial}{\partial\beta}\Big|_{\beta=\alpha}I_k(\alpha,\beta;\tau),\qquad J_k'(\alpha,\alpha;\tau)=\frac{\partial}{\partial\beta}\Big|_{\beta=\alpha}J_k(\alpha,\beta;\tau),$$

and obtain

$$(I_1'+I_3')(\alpha,\alpha;\tau)=0\ ,$$
$$I_2'(\alpha,\alpha;\tau)=\frac{1}{\tau\sqrt{\alpha^2+4}}K(m_2)\ ,$$
$$(J_1'+J_3')(\alpha,\alpha;\tau)=\frac{\alpha}{\tau^2-\alpha^2}\frac{2}{\sqrt{\tau^2+4}}\Big(\bar{K}(m_1)-\frac{\tau^2+4}{\alpha^2+4}\bar{E}(m_1)\Big)\ ,$$
$$J_2'(\alpha,\alpha;\tau)=\frac{2}{\tau\sqrt{\alpha^2+4}}\Big(\frac{\tau^2}{\tau^2-\alpha^2}E(m_2)-\frac{1}{2}K(m_2)\Big)\ .$$

Finally, by l'Hôpital,

$$\lim_{a\to b}\tilde{Q}(\alpha,\beta;\tau)=\frac{\partial Q}{\partial\beta}\Big|_{\alpha=\beta}$$
$$=\frac{\tau^2}{\alpha^2}\frac{\tau}{\tau^2-\alpha^2}\sqrt{\frac{\alpha^2+4}{\tau^2+4}}\frac{\bar{K}(m_1)E(m_2)+m_2\bar{E}(m_1)K(m_2)-\bar{K}(m_1)K(m_2)}{K(m_2)^2}.$$

Now note that the function $\tilde{Q}$ can be extended to a holomorphic function of complex arguments α,β,τ. The computation above shows that it remains bounded for $\alpha=\beta$, and hence extends holomorphically to $\alpha=\beta$. In particular, the extension for real arguments is real analytic. □

The solution set to (5.1) is shown in Figure 5.1. In Figure 5.2, we show two surfaces in the intersection with extreme values of α. In the next section, we will analyze the Traizet limit on the right (with small α). The left image strongly suggest that, in the limit of large α, the family tends to a doubly periodic Karcher-Meeks-Rosenberg surface of genus 1 [Kar88, Kar89, MR89].

6. Revisiting the Traizet limit

With our parametrization of oH, the Traizet limit, with infinitesimally small catenoid nodes, corresponds to the limit $ab\to 1$ or $\alpha+\beta\to 0$. In this limit, the Gauss map $G(z)=i$ except at two singular points $z=1/a=b$ and $z=-a=-1/b$.

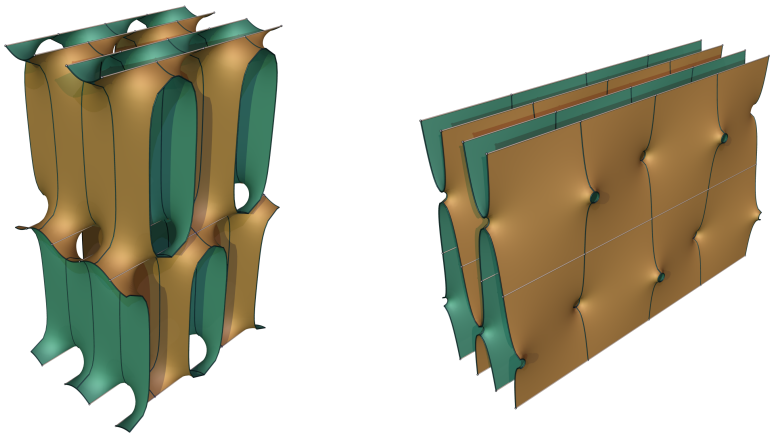

FIGURE 5.2. Two surfaces in the intersection of $\overline{\mathrm{oH}} \cap \mathrm{oP}$

So the octagon degenerates into the plane $y = 0$ as expected. The angle of the limit rhombic torus can be computed as

$$\tan\frac{\theta}{2} = \frac{|\int_{-1/t}^{1/t} dh|}{|\int_{1/t}^{t} dh|} = \frac{K'(m)}{K(m)}, \tag{6.1}$$

where $m = \tau^2/(\tau^2+4)$.

From (5.1), we can already locate the Traizet limit of $\overline{\mathrm{oH}} \cap \mathrm{oP}$. First note that $m_2 \to 0$ when $\alpha = \beta \to 0$. Divide both sides of (5.1) by m_2 to eliminate the trivial but meaningless solution at $\alpha = \beta = 0$. Recall that [BF71] $(K(m) - E(m))/m \to \pi/4$ and $K(m) \to \pi/2$ as $m \to 0$. Hence we obtain for the Traizet limit

$$2E(m) = K(m),$$

where $m = \tau^2/(\tau^2+4)$. This is uniquely solved with $\tau \approx 4.35932$ or $t \approx 4.57777$. By putting these parameters into (6.1), we recover the angle

$$\theta^* \approx 1.23409 \approx 70.7083^\circ.$$

While we did not manage to prove uniqueness Conjecture 4.3, we can however prove the uniqueness at the Traizet limit.

Theorem 6.1. *For any $0 < \theta < \theta^*$, there is a non-trivial solution $0 < x < 1/2$ that solves the balance equation (1.2). This solution is unique and non-degenerate, hence is the Traizet limit for a family of TPMS.*

Proof. Recall that $T_{1,2} = \exp(\pm i\theta/2)$ and $T_3 = -T_1 - T_2 = -2\cos(\theta/2)$. We consider the function

$$f(x;\theta) = x\eta_3(\theta) - \zeta(xT_3(\theta);\theta).$$

Observe the following properties of f.

- $f \to +\infty$ as $x \to 0+$. To see this, note that the lattice is spanned by conjugate vectors T_1, T_2, so $\zeta(z)$ is real for real z. By definition, it has residue $+1$ at 0. The claim follows.
- $\partial_x^2 f > 0$ for $0 < x < 1/2$. This can be seen by noting that
$$\frac{\partial^2 f}{\partial x^2} = T_3^2 \wp'(xT_3)$$
is clearly non-zero. So f must be convex in x.

So there is a unique non-trivial solution of $f(x) = 0$ if

$$g(\theta) := \frac{\partial f}{\partial x}\Big|_{x=1/2} = T_3 \wp(T_3/2) + \eta_3 > 0,$$

or no non-trivial solution otherwise. These two cases are separated by the zeroes of $g(\theta)$. They correspond to the Traizet limit of $\overline{\text{oH}} \cap \text{oP}$, which is uniquely given by θ^*. Since non-trivial solutions are known for $\theta = \pi/3 < \theta^*$, we conclude that $g(\theta) > 0$ if and only if $0 < \theta < \theta^*$.

For the non-degeneracy, we consider the function

$$F(x, y; \theta) = (x + y)\eta_1(\theta) + (x - y)\eta_2(\theta) - \zeta((x + y)T_1(\theta) + (x - y)T_2(\theta); \theta) \ .$$

Note that $F(x, 0; \theta) = -f(x, \theta)$. So the convexity of f in x implies that $\partial_x F(x, 0; \theta)$ is real negative at a non-trivial solution of (1.2). On the other hand

$$\frac{\partial F}{\partial y}\Big|_{y=0} = \eta_1 - \eta_2 + (T_1 - T_2)\wp(xT_3)$$

is positive purely imaginary for $0 < x < 1/2$. This can be seen by noting that

$$\frac{\partial}{\partial x}\frac{\partial F}{\partial y}\Big|_{y=0} = (T_2^2 - T_1^2)\wp'(xT_3)$$

is negative purely imaginary for $0 < x < 1/2$, and $\partial_y F$ is positive purely imaginary at $(x, y) = (1/2, 0)$. The non-degeneracy then follows readily. □

Note that, as θ approaches θ^*, the non-trivial solution tends to $1/2$, and $T_3\wp(T_3/2)+\eta_3$ tends to 0. So the balanced configuration at $(x, \theta) = (1/2, \theta^*)$ is degenerate.

We may also recover solutions of (1.2) in terms of our parametrization.

Proposition 6.2. *The Traizet limit of* oH *is described by the equation*

$$(2\beta^2 - \tau^2 + 4)K(m) = 2(\beta^2 + 4)\Pi(n, m), \tag{6.2}$$

where $\Pi(n, m)$ *is the complete elliptic integral of the third kind, with the characteristic* $n = \tau^2/(\tau^2 - \beta^2) > 0$*, and the modulus* $m = \tau^2/(\tau^2 + 4)$*.*

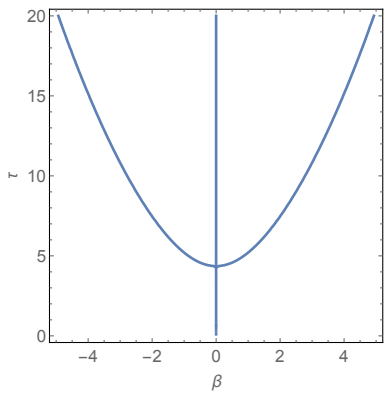

FIGURE 6.1. Solution set (β, τ) to the period condition (6.2) describing the Traizet limit of oH, together with the trivial locus $\beta = 0$ describing the Traizet limit of oP. To compare with Figure 1.4.

Proof. Again, with the help of the integral tables in [BF71], we obtain $I_2(-\beta,\beta;\tau) = J_2(-\beta,\beta;\tau) = 0$ and

$$(I_1+I_3)(-\beta,\beta;\tau) = (J_1+J_3)(-\beta,\beta;\tau) = \sqrt{1-m}K(m)\ ,$$

and the derivatives up to order 2 with respect to α at $\alpha=-\beta$

$$(I_1'+I_3')(\alpha,\beta;\tau) = (J_1'+J_3')(\alpha,\beta;\tau) = \frac{\beta}{\tau^2-\beta^2}\frac{1}{\sqrt{\tau^2+4}}\Pi(n,m)\ ,$$

$$I_2'(\alpha,\beta;\tau) = J_2'(\alpha,\beta;\tau) = \frac{\pi}{2}\frac{1}{\sqrt{(\tau^2-\beta^2)(\beta^2+4)}}\ ,$$

$$I_2''(\alpha,\beta;\tau) = J_2''(\alpha,\beta;\tau) = \frac{\pi}{2}\frac{\beta}{\sqrt{(\tau^2-\beta^2)(\beta^2+4)}}\Big(\frac{1}{\tau^2-\beta^2}-\frac{1}{\beta^2+4}\Big).$$

We look at a modified period condition, namely

$$\hat{Q} = \frac{1/Q_I - 1/Q_J}{(\alpha+\beta)^2} = 0\ .$$

The evaluations above suffice to compute, by l'Hôpital, that

$$\lim_{\alpha\to-\beta+}\hat{Q}(\alpha,\beta;\tau) = \frac{\partial^2}{\partial\alpha^2}\Big|_{\alpha=-\beta}(1/Q_I-1/Q_J)$$
$$= \frac{\pi\beta\sqrt{\tau^2+4}}{4(\beta^2+4)^{3/2}(\tau^2-\beta^2)^{3/2}}\frac{(2\beta^2-\tau^2+4)K(m)-2(\beta^2+4)\Pi(n,m)}{K(m)^2}.$$

Hence $\hat{Q}$ extends analytically to $\alpha+\beta=0$. Under the constraint $\tau>\beta$, we notice indeed two loci: $\beta=0$ for the Traizet limit of oP, and the Traizet limit of oH must be described by (6.2). □

And (6.2) must be describing the unique non-trivial locus of (1.2). Its solution set is plotted in Figure 6.1. Alternatively, (6.2) can also be written in the forms

$$(\tau^2+4)K(m) = 2(\beta^2+4)\Pi(n',m)$$

where $n' = (\tau^2-\beta^2)/(\tau^2+4)$, or

$$\Big(8\frac{\tau^2}{n''}+(\tau^2-4)(\beta^2+4)\Big)K(m) = 8\Big(\frac{\tau^2}{n''}-(\beta^2+4)\Big)\Pi(n'',m)$$

where $n'' = \beta^2/(\beta^2+4)$.

To find the intersection with the trivial locus, let $\beta\to 0+$. For the three forms of (6.2), we recall, respectively, that

$$\lim_{n\to1+}\Pi(n,m) = K(m) - \frac{E(m)}{1-m} \qquad \text{[DLMF, (19.6,6)]};$$

$$\lim_{n'\to m}\Pi(n',m) = \frac{E(m)}{1-m} \qquad \text{[DLMF, (19.6.1)]};$$

$$\lim_{n''\to0+}\frac{\Pi(n'',m)-K(m)}{n''} = \frac{K(m)-E(m)}{m} \qquad \text{cf. [BF71, (733.00)]}.$$

Any one of these leads once again to

$$2E(m) = K(m).$$

Remark 6.3. The magic equation $2E(m)=K(m)$ also appeared in [CW18] for locating the bifurcation point in the tD family.

Remark 6.4. Assume that the limit torus is spanned by $T_1=1$ and $T_2=\tau$. We have studied the rhombic case $|\tau|=1$. Numerically, we find that if τ is taken from the colored region on the left in Figure 6.2, within the fundamental domain of the modular group, then there is unique non-trivial position $p_2(\tau)$ that solves

Traizet's balance equation (1.1). The left boundary curve of this region, which is asymptotic to the circle $|z-1|=1$ as $|\tau|\to 0$, represents a one-parameter family of tori for which the trivial configuration $x=y=1/2$ is degenerate. The image of the continuous map $\tau\mapsto p_2(\tau)$ is the colored region on the right in Figure 6.2. The coloring should help to visualize the map.

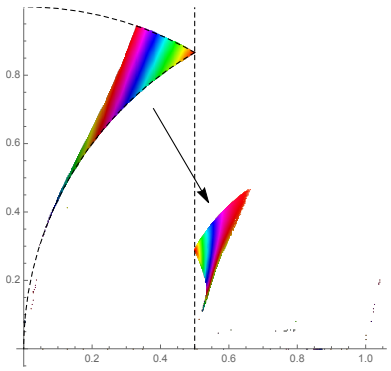

FIGURE 6.2.

Remark 6.5. It recently comes to our attention that the solutions of Traizet's balance equation (1.1) have been systematically studied in the PDE contexts as the critical points of the Green function on flat tori [LW10, CKLW18, BE16]. For a fixed torus, apart from the trivial solutions at the 2-division points, there could be at most one pair of non-trivial solutions. In other words, the balancing equation has either three or five solutions. The boundary between the two cases provides a 1-parameter family of degenerate balanced configuration.

Let k_r denote the r-th *elliptic integral singular values*, i.e. $K'(k_r^2)/K(k_r^2)=\sqrt{r}$. A table of k_r can be found in [Bow61, p. 95] and [BB87, (4.6.10)].

It was calculated by Legendre (see [WW62, §22.81]) that $k_3=(\sqrt{6}-\sqrt{2})/4$, hence $K'(m)/K(m)=1/\sqrt{3}$ when $m=1-k_3^2=(2+\sqrt{3})/4$. We then see from (6.1) that the rhombic torus with $\theta=60^\circ$ occurs when $\tau=2(2+\sqrt{3})$. Then (6.2) is solved, very conveniently, with $\beta=2$. One then verifies that the singular point at β is mapped to one third of the height of the box. These are then explicit parameters for the Traizet limit of Schwarz' H family.

We are now ready to prove:

Theorem 6.6. *Schwarz* H *surfaces can be deformed within the set of TPMS of genus three into Meeks surfaces.*

Proof. Within a sufficiently small neighborhood of a Traizet limit, Traizet's construction actually implies a homeomorphism between the space of TPMS of genus three and the space of 3-tori. This was not explicitly stated in [Tra08], but follows from his design of the Weierstrass data and the uniqueness in the implicit function theorem, as argued in [Tra02]. Let U be such a neighborbood of the Traizet limit of H. In particular, $U\cap$ oH is connected.

Now fix $\epsilon>0$. We consider the oH surfaces with $\alpha+\beta=\epsilon$. The period condition for such surfaces is $\tilde{Q}_\epsilon(\beta,\tau)=\tilde{Q}(\epsilon-\beta,\beta;\tau)=0$, defined on the region $\{(\beta,\tau)\in\mathbb{R}^2_+ : \tau>\beta\geq\epsilon/2\}$. We have shown that $\tilde{Q}_\epsilon(\beta;\tau)$ is negative as τ approaches β, and positive as τ tends to infinity. This holds, in particular, also for $\alpha=\beta=\epsilon/2$. Hence in the real analytic solution set of $\tilde{Q}_\epsilon=0$, there must be a

real analytic curve γ that separates the line $\tau = \beta$ from $\tau = \infty$. If ϵ is sufficiently small, the curve γ passes through U.

So we deform an H surface first along the H family into U, then within $U \cap$ oH onto the curve γ, finally along γ until an oP surface. The latter belongs to Meeks, which is connected. Note that this deformation path is within oH until hitting oP. □

Remark 6.7. It is easy to find $k_1 = 1/\sqrt{2}$, hence $K'(m)/K(m) = 1$ when $m = 1 - k_1^2 = 1/2$. We then see from (6.1) that the rhombic torus becomes square when $\tau = 2$. In this case, (6.2) has no solution with $\beta < \tau$. So the only balanced configuration is with $\beta = 0$. This is the Traizet limit of the tetragonal deformation family tP of Schwarz' P surface.

References

[BB87] Jonathan M. Borwein and Peter B. Borwein. *Pi and the AGM*. Canadian Mathematical Society Series of Monographs and Advanced Texts. John Wiley & Sons, Inc., New York, 1987. A study in analytic number theory and computational complexity, A Wiley-Interscience Publication.

[BE16] Walter Bergweiler and Alexandre Eremenko. Green's function and anti-holomorphic dynamics on a torus. *Proc. Amer. Math. Soc.*, 144(7):2911–2922, 2016.

[BF71] Paul F. Byrd and Morris D. Friedman. *Handbook of elliptic integrals for engineers and scientists*. Die Grundlehren der mathematischen Wissenschaften, Band 67. Springer-Verlag, New York-Heidelberg, 1971. Second edition, revised.

[Bow61] F. Bowman. *Introduction to elliptic functions with applications*. Dover Publications, Inc., New York, 1961.

[CKLW18] Zhijie Chen, Ting-Jung Kuo, Chang-Shou Lin, and Chin-Lung Wang. Green function, Painlevé VI equation, and Eisenstein series of weight one. *J. Differential Geom.*, 108(2):185–241, 2018.

[CW18] Hao Chen and Matthias Weber. A new deformation family of schwarz' d surface. page 15 pp., 2018. preprint, `arXiv:1804.01442`.

[DLMF] *NIST Digital Library of Mathematical Functions*. http://dlmf.nist.gov/, Release 1.0.19 of 2018-06-22. F. W. J. Olver, A. B. Olde Daalhuis, D. W. Lozier, B. I. Schneider, R. F. Boisvert, C. W. Clark, B. R. Miller and B. V. Saunders, eds.

[FH92] Andrew Fogden and Stephen T. Hyde. Parametrization of triply periodic minimal surfaces. II. regular class solutions. *Acta Cryst. Sect. A*, 48(4):575–591, 1992.

[FH99] Andrew Fogden and Stephan T. Hyde. Continuous transformations of cubic minimal surfaces. *The European Physical Journal B-Condensed Matter and Complex Systems*, 7(1):91–104, 1999.

[FHL93] Andrew Fogden, M. Haeberlein, and Sven Lidin. Generalizations of the gyroid surface. *J. Phys. I*, 3(12):2371–2385, 1993.

[FK89] Werner Fischer and Elke Koch. Genera of minimal balance surfaces. *Acta Cryst. Sect. A*, 45(10):726–732, 1989.

[HKW99] David Hoffman, Hermann Karcher, and Fusheng Wei. The singly periodic genus-one helicoid. *Comment. Math. Helv.*, 74(2):248–279, 1999.

[Kar88] H. Karcher. Embedded minimal surfaces derived from Scherk's examples. *Manuscripta Math.*, 62(1):83–114, 1988.

[Kar89] Hermann Karcher. Construction of minimal surfaces. *Surveys in geometry*, pages 1–96, 1989.

[LL90] Sven Lidin and Stefan Larsson. Bonnet transformation of infinite periodic minimal surfaces with hexagonal symmetry. *Journal of the Chemical Society, Faraday Transactions*, 86(5):769–775, 1990.

[LW10] Chang-Shou Lin and Chin-Lung Wang. Elliptic functions, Green functions and the mean field equations on tori. *Ann. of Math. (2)*, 172(2):911–954, 2010.

[Mee90] William H. Meeks, III. The theory of triply periodic minimal surfaces. *Indiana Univ. Math. J.*, 39(3):877–936, 1990.

[MR89] William H. Meeks, III and Harold Rosenberg. The global theory of doubly periodic minimal surfaces. *Invent. Math.*, 97(2):351–379, 1989.

[Sch90] Hermann A. Schwarz. *Gesammelte Mathematische Abhandlungen*, volume 1. Springer, Berlin, 1890.

[Sch70] Alan H. Schoen. Infinite periodic minimal surfaces without self-intersections. Technical Note D-5541, NASA, Cambridge, Mass., May 1970.

[Tra02] Martin Traizet. Adding handles to Riemann's minimal surfaces. *J. Inst. Math. Jussieu*, 1(1):145–174, 2002.

[Tra08] Martin Traizet. On the genus of triply periodic minimal surfaces. *J. Differential Geom.*, 79(2):243–275, 2008.

[Wey06] Adam G. Weyhaupt. *New families of embedded triply periodic minimal surfaces of genus three in euclidean space*. ProQuest LLC, Ann Arbor, MI, 2006. Thesis (Ph.D.)–Indiana University.

[Wey08] Adam G. Weyhaupt. Deformations of the gyroid and Lidinoid minimal surfaces. *Pacific J. Math.*, 235(1):137–171, 2008.

[WHW09] Matthias Weber, David Hoffman, and Michael Wolf. An embedded genus-one helicoid. *Ann. of Math. (2)*, 169(2):347–448, 2009.

[WW62] E. T. Whittaker and G. N. Watson. *A course of modern analysis. An introduction to the general theory of infinite processes and of analytic functions: with an account of the principal transcendental functions*. Fourth edition. Reprinted. Cambridge University Press, New York, 1962.

(Chen) Georg-August-Universität Göttingen, Institut für Numerische und Angewandte Mathematik

Email address: h.chen@math.uni-goettingen.de

(Weber) Indiana University, Department of Mathematics

Email address: matweber@indiana.edu